JOURNAL OF SOLID STATE CHEMISTRY 119, 281–288 (1995)

In Situ Study of the Phase Transition in $Bi_2Ti_4O_{11}$

L. Nistor,*,[1] G. Van Tendeloo,*,[2] S. Amelinckx,* V. Kahlenberg,† and H. Böhm‡

*EMAT, University of Antwerp (RUCA), Groenenborgerlaan 171, B-2020 Antwerp, Belgium; †Technische Universität Berlin, Institut für Mineralogie/Kristallographie, Ernst Reuter Platz 1, Germany; and ‡Johannes Gutenberg-Universität, Institut für Geowissenschaften, FB 22, D-55099 Mainz, Germany

Received February 22, 1995; accepted May 16, 1995

DEDICATED TO PROF. DR. WOLFRAM PRANDL ON THE OCCASION OF HIS 60TH BIRTHDAY

The paraelectric ↔ antiferroelectric phase transition of the compound $Bi_2Ti_4O_{11}$ is studied *in situ* by electron diffraction and electron microscopy. The transition is reversible and clearly second order. Above T_c faint streaking at the superlattice positions persists. In the low-temperature phase, antiphase boundaries with a displacement vector R = 1/2[101] are revealed; they show a finite width, suggesting a gradual displacement of the Bi atoms at the transition. A model for the domain wall configuration is proposed, based on the influence of the lone pairs of Bi^{3+} ions at the transition.

INTRODUCTION

The room temperature crystal structure of α-$Bi_2Ti_4O_{11}$ as determined by Petrushkova *et al.* (1) and refined by Kahlenberg and Böhm (2) is monoclinic with lattice parameters a = 1.45999 nm, b = 0.38063 nm, c = 1.49418 nm, β = 93.1288°, and space group $C2/c$. It consists of double chains of deformed TiO_6 octahedra running parallel to the [010] direction and interlinked partially by edge-sharing and partially by corner-sharing. These octahedra build up a network with channels along [010] in which the Bi atoms are placed. At a temperature of about 506 K α-$Bi_2Ti_4O_{11}$ undergoes a reversible paraelectric to antiferroelectric phase transition, which has been observed by several authors using different methods: dielectric and dilatational measurements (3), Raman scattering experiments (4), X-ray diffraction (5, 6), and linear excess birefringence (6). A detailed structural description of the transformation was given in (2). The transition is induced by very small (0.029 nm) displacements of the Bi cations in the TiO_6 octahedral network, whereas Ti and O atoms remain at their positions. The shifts of the Bi atoms are parallel and antiparallel to the b axis. The lattice parameters of the high-temperature β-phase are a' = 1.46412 nm, b' = 0.38032 nm, c' = 1.07824 nm, and β = 136.1350°; its space group is $C2/m$.

The transition from the high-temperature to the low-temperature phase is characterized by the loss in translational symmetry (2). Consequently, the occurrence of antiphase boundaries is to be expected in the α-phase. Transmission electron microscopy and electron diffraction are useful methods for a study of phase transitions because it is possible to observe microstructural transformations when varying the sample temperature. As yet $Bi_2Ti_4O_{11}$ crystals were never examined by electron microscopy; it is the purpose of this paper to investigate *in situ* the phase transformation and to characterize its microstructure by high resolution electron microscopy.

EXPERIMENTAL

Needle-shaped single crystals of α-$Bi_2Ti_4O_{11}$ were grown from a flux at the Institut für Geowissenschften in Mainz, by a method described in (2). Samples for transmission electron microscopy were prepared by crushing the crystallites and gluing the fragments to microscope copper grids. Ion beam thinning of needle-shaped single crystals or of pieces cleaved perpendicular to the needle axis was also tried, but these specimens could not be oriented in the microscope along the zone axes of interest for studying the phase transition. The phase transition was studied *in situ* using a double tilt heating holder in a Philips CM-20 electron microscope. High resolution electron microscopy at room temperature was performed using a JEOL-4000EX electron microscope.

RESULTS

Electron Diffraction

Figure 1 shows several sections of reciprocal space of the α-phase taken at room temperature. The indices refer to the pseudotetragonal unit cell with β = 93°. In the

[1] On leave from the Institute of Atomic Physics, P.O. Box Mg-6 Magurele, Bucharest, Romania.

[2] To whom correspondence should be addressed.

0022-4596/95 $12.00

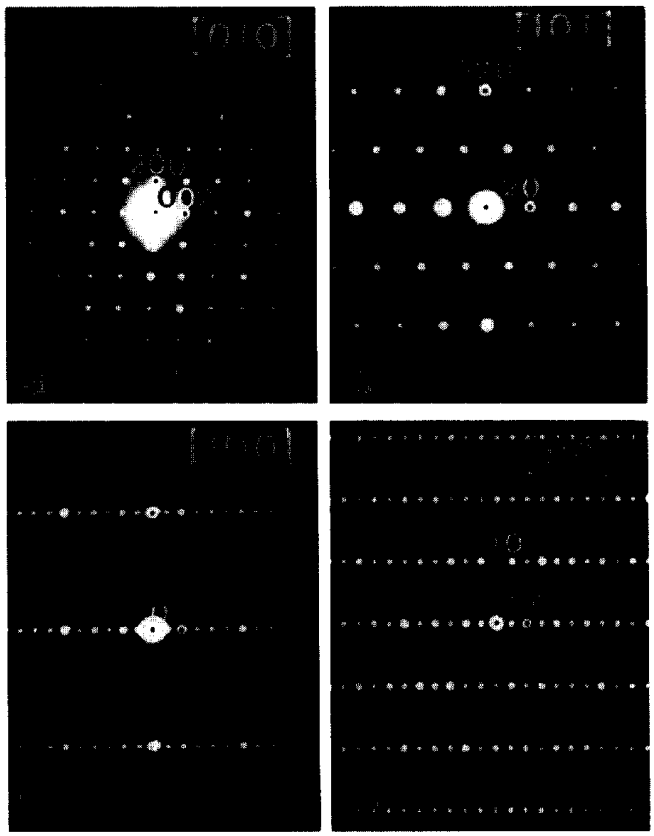

FIG. 1. Electron diffraction patterns of α-$Bi_2Ti_4O_{11}$ along different directions: (a) [010]; (b) [101]; (c) [100]; (d) [110].

electron diffraction patterns from Figs. 1a and 1b all diffraction spots are sharp and have comparable intensities. They suggest the following diffraction conditions:

$$hkl: \quad h + k = \text{even}$$
$$00l: \quad l = \text{even}$$
$$h0l: \quad h = \text{even and } l = \text{even}$$
$$0k0: \quad k = \text{even}.$$

These conditions are consistent with the $C2/c$ space group determined by X-ray diffraction (2) for the low temperature α-phase. In the diffraction patterns of Figs. 1c and 1d two families of reflections are present:

$$\text{intense}, \quad \text{for } h + l = \text{even and}$$
$$\text{weak}, \quad \text{for } h + l = \text{odd}.$$

The weak reflections along the $[00l]^*$ reciprocal row, which appear at extinct positions, can be shown to arise from double diffraction.

Electron diffraction patterns along several zone axes were obtained at room temperature, at temperatures in the vicinity of the transition, and above. Since one measures the temperature of the furnace and not of the sample, a deviation of several K from the displayed values is possible. Such a deviation also arises because of differences in the thermal contact of different crystallites with the copper grid.

Gradually heating the sample in the heating holder causes no significant changes in the diffraction patterns until approximately 30 K below the α–β transition temperature; then the intensity of all weak spots gradually drops, but it does not vanish completely, even at temperatures 50–100 k above T_c. The intensity, however, becomes very faint and only elongated streaks along the c^* direction persist. The "basic" reflections remain sharp and round, and their intensity does not noticeably change. The transition is reversible, and on cooling below T_c the intensity of the weak spots is gradually recovered; finally the characteristic low-temperature phase diffraction pattern is restored. The evolution of the diffraction patterns through the transition temperature is illustrated in Fig. 2 for the [110] and [130] zones. The gradual change of the weak spot intensity is evident. At temperatures of approximately 540 K for the [110] zone and 570 K for the [130] zone, very faint streaking along c^* can still be observed in the diffraction patterns (Figs. 2c and 2f).

In the [010] zone diffraction pattern no superstructure spots are present and therefore no changes were observed as function temperature. This is clearly consistent with the assumption that the transition is attributed to atom displacements along the [010] direction (2).

Electron Microscopy

For a more complete structural characterization of the α-$Bi_2Ti_4O_{11}$ phase, high resolution bright field electron microscopy was performed at room temperature. The most favorable orientation to reveal the geometry of the structure in a 2-D image is along the [010] zone axis. A schematic projection of the structure along this zone is given in Fig. 3. It shows the linkage of the deformed TiO_6 octahedra to form the walls of the channels in which pairs of Bi atoms are placed. Figure 4 is a high resolution image along the [010] zone, obtained from the thinnest part of the specimen; it reveals all the heavy atom columns as dark dots. The pairs of Bi columns appear as the darker dots, while the six pairs of Ti columns surrounding them are imaged as less dark dots. The image can be compared directly with the model of the structure given in Fig. 3. The unit cell is marked. The four pairs of Bi columns can easily be recognized. In the high resolution image not only the geometry of the black dot pattern but also the scale is in complete accordance with the structure determination. For instance, in this projection, the distance

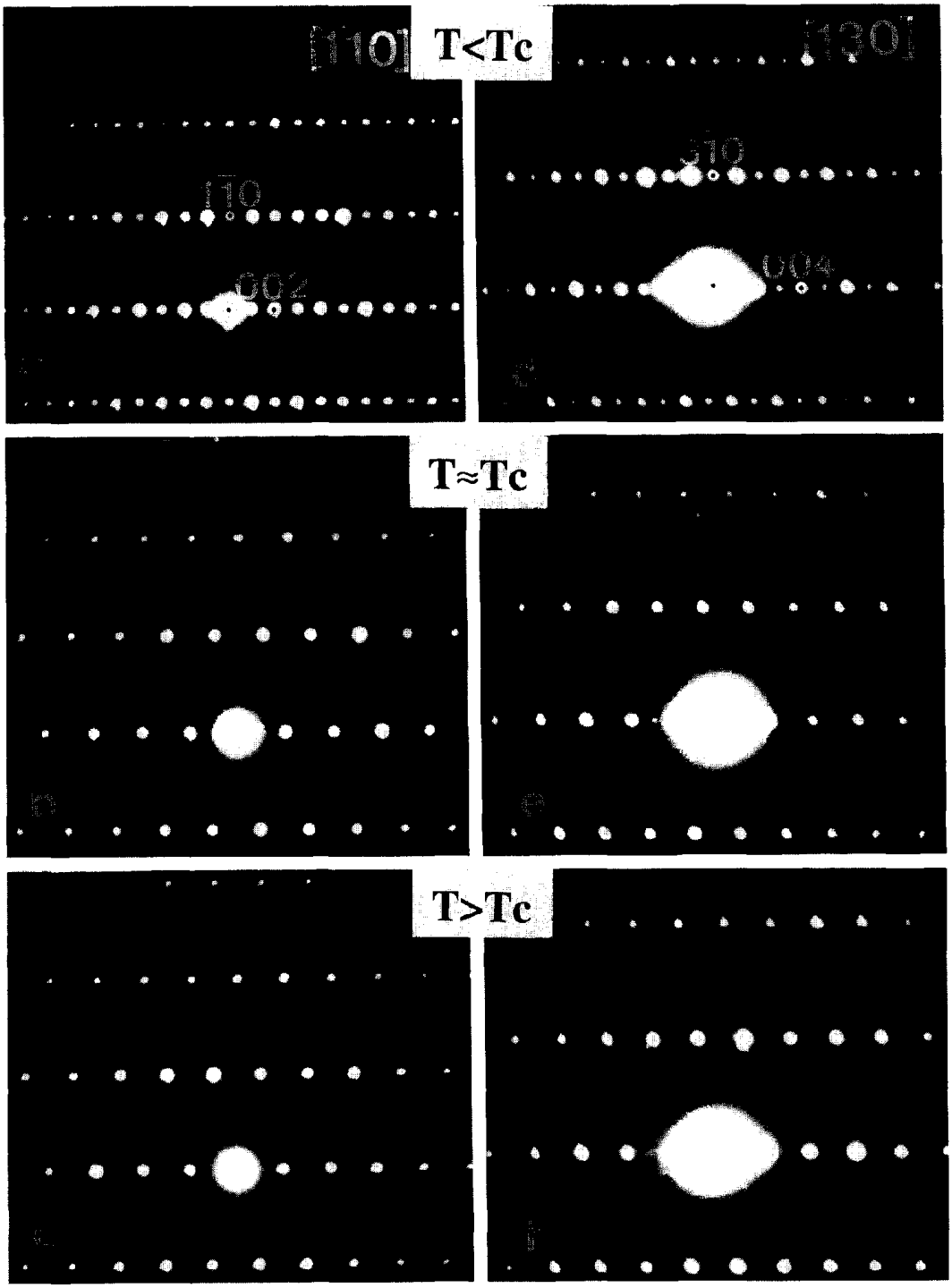

FIG. 2. Temperature evolution of the [110] pattern (left) and the [130] diffraction pattern (right) from room temperature until above T_c.

between the two Bi columns in a pair is 0.30 nm while the shortest distances between Ti columns are 0.23 or 0.20 nm. Oxygen atoms are not revealed as separate columns. No planar defects are detected in this projection.

Figure 5 shows a high resolution image of the α-$Bi_2Ti_4O_{11}$ phase along the [110] zone, which reveals the stacking of the layers of cations pairs. Heavy atom columns are imaged as black dots. The unit cell is indicated in the figure. The marked succession of the pairs of cation columns is the following: Ti–Bi, Ti–Bi, Ti–Ti, Ti–Bi,

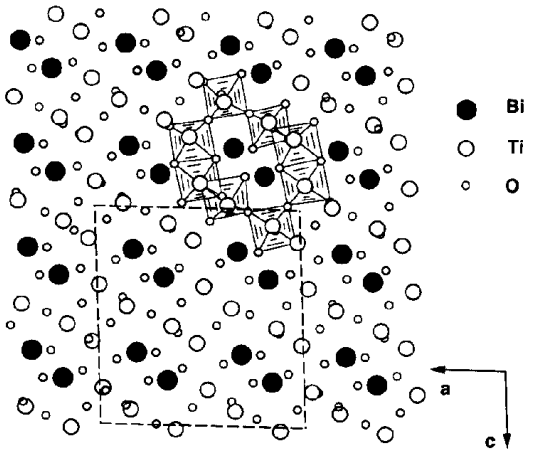

FIG. 3. Schematic structural representation of α-$Bi_2Ti_4O_{11}$ projected along the *b* axis. The darker dots are the Bi atoms, the lighter are Ti, and the small dots represent oxygen. The unit cell is indicated by dashed lines.

Ti–Bi, Ti–Ti, Ti–Bi. The pairs of columns are imaged as single dots. The Ti–Ti pairs show a lighter contrast under the used imaging conditions.

Since the structure of $Bi_2Ti_4O_{11}$ is rather complex, large variations in the high resolution image contrast were observed with small defocusing and small changes in specimen thickness. Image simulations were essential in order to support the interpretation of the high resolution images. The simulations were performed with the "Mac Tempas" software package. Images were computed for different thicknesses and defocusing values. The microscope parameters used were the following: accelerating voltage V = 400 kV, spherical aberation constant C_s = 1 mm, beam divergence θ = 0.6 mrad, and focus spread Δ = 10 nm. The calculated image matrices for the [010] and [110] zones are reproduced, respectively in Figs. 6a and 6b. The best fit is obtained for small thicknesses (2–4 nm) and defocusing conditions close to Scherzer value. The high resolution images confirm the model of the structure determined by X-ray diffraction on α-$Bi_2Ti_4O_{11}$ single crystals (2).

Since the paraelectric–antiferroelectric transition is associated with displacements of Bi atoms parallel to the unique [010] direction, no orientation domains are expected. However, since translation symmetry is lost, antiphase boundaries may result. The displacement vector is $\mathbf{R} = 1/2[101]_{pt}$ (i.e., the lost symmetry translation); the index "pt" means pseudotetragonal (i.e., the *hkl* indices

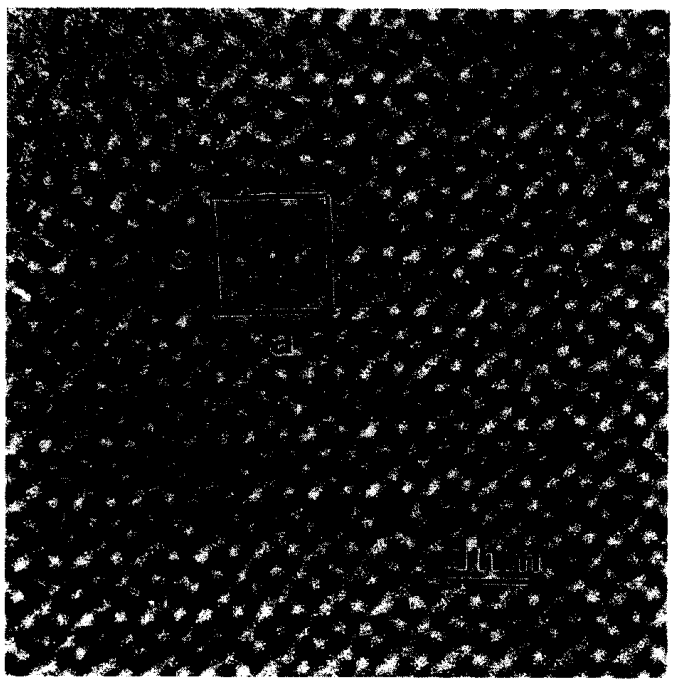

FIG. 4. High resolution image of $Bi_2Ti_4O_{11}$ along [010]; there is a one-to-one correspondence between the dark dots in this image and the metal ion configuration in the structural representation of Fig. 3.

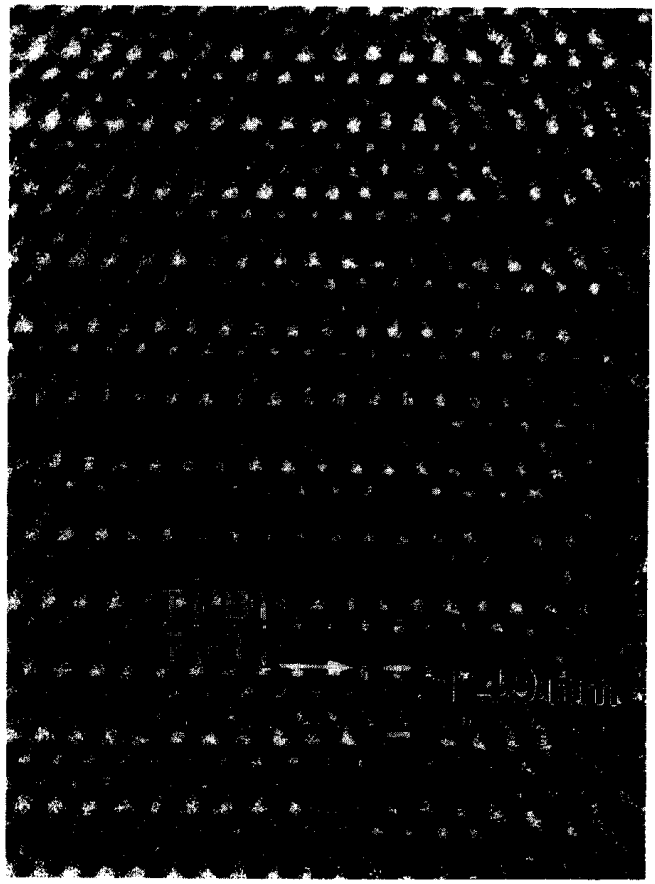

FIG. 5. HREM image along [110]. Different layers can be discerned.

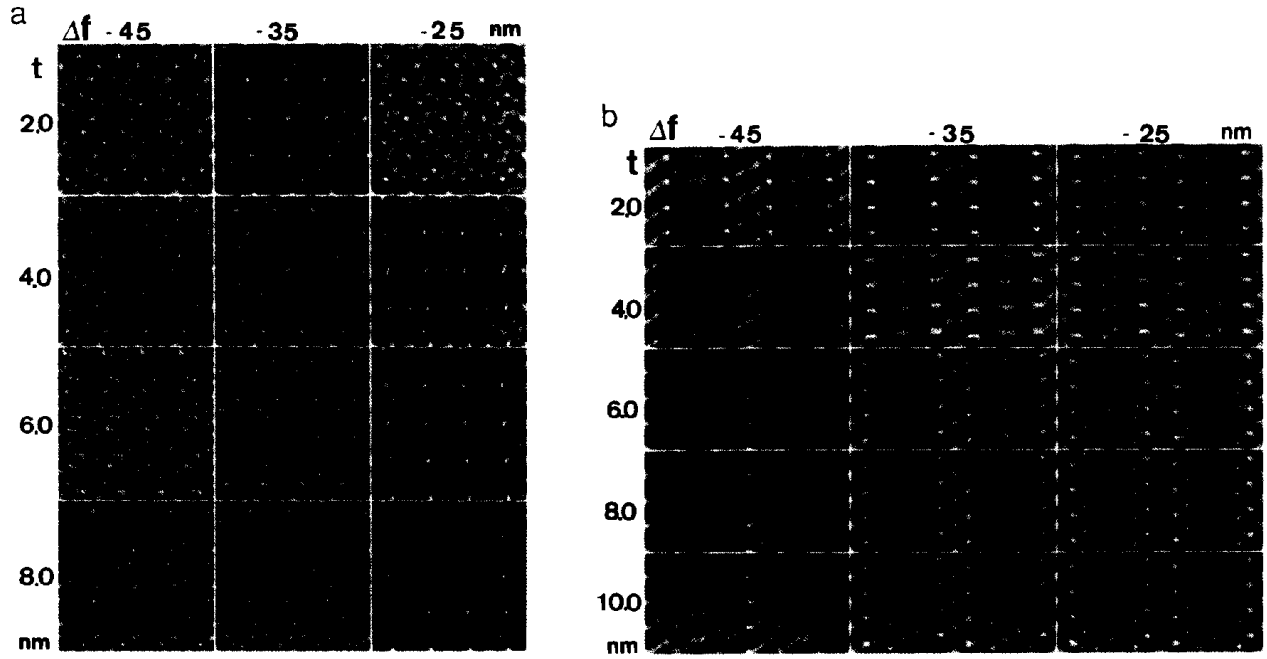

FIG. 6. Calculated HREM images as function of defocus value (Δf) and thickness (t) for the microscope parameters of the 4000EX. (a) Along [010]; (b) along [110].

refer to the pseudotetragonal unit cell). This translation relates the structure factors in the two domains by a phase factor $\exp i\alpha = \exp 2\pi i\mathbf{g}\cdot\mathbf{R} = \exp \pi i(h + l)$. It is therefore evident that only for reflections with $h + l$ = odd, the interfaces can be imaged by diffraction contrast as α-fringes, with a phase shift $\alpha = \pi$. Two beam dark-field diffraction contrast images in a superstructure spot (i.e., with $h + l$ = odd) could in principle reveal the interfaces as α-fringes ($\alpha = \pi$). However, since the Bi displacements are small, the extinction distances associated with superstructure reflections are large and presumably larger than the foil thickness. Only a weak line contrast is to be expected. In practice, in the present case this method proved to be inadequate.

More successful in demonstrating the presence of antiphase boundaries was lattice fringe imaging. However, when applying this method one has to be aware that lattice fringes are not only shifted at translation interfaces but also on crossing inclination contours and equal thickness fringes. For lattice fringe imaging two adjacent reflections (strong–weak) or three adjacent reflections (weak–strong–weak) of the type described before could be used. Since the superlattice reflections are extinct in the $00l$ row, one has to use a noncentral hkl row. The [010] zone has to be excluded, since all displacements of the Bi atoms are along the [010] zone axis. To enhance the image contrast, the sample was tilted in such a way that the Ewald sphere intersects the chosen reciprocal lattice nodes; the corresponding reflections will then exhibit enhanced intensity. Even under these particular imaging conditions, in which interfaces appear in an easily readable contrast, antiphase boundaries were only occasionally observed and were rather singular within one crystallite. Since in the present study we used crushed samples with crystallites of dimensions in the range of 10 μm, it is plausible that the crystallites were too small and many of them single domains.

Figure 7a exhibits a dark field lattice fringe image obtained with three adjacent reflections (weak–strong–weak) of an α-$Bi_2Ti_4O_{11}$ crystallite. For dark-field imaging the sample was tilted a few degrees away from the [170] zone axis. The image shows an antiphase boundary which appears as a zig zag-shaped darker band. The contrast of the domains is the same on both sides of the interface, proving that the two domains are geometrically related by a translation. At high magnification (Fig. 7b) the fringe pattern is better evidenced. It consists of an alternation of strong and weak bright fringes, with the period of 1.49 nm. The strong fringes result mainly from the interference between the strong central spot and one adjacent weak spot. The weak fringes result mainly from the interference between the two outer weak spots. Their spacing is in fact half of that of the strong fringes, but every other of these weak fringes coincides with a strong fringe. Note that the weak fringes have the same spacing as the strong ones, but that they are not positioned exactly midway between two strong fringes. This can be understood by noting that the position of lattice fringes depends on the *s*-

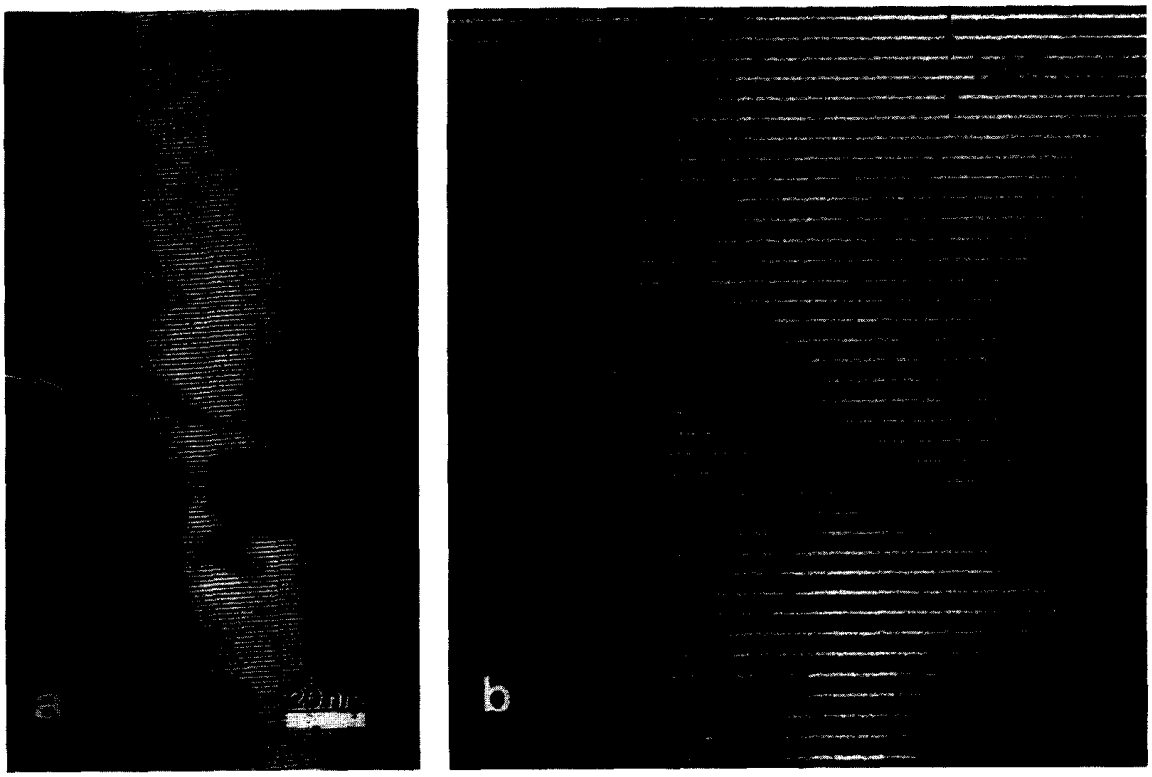

FIG. 7. Dark field images corresponding to a [$hk0$] section, selecting two off-central weak α-phase reflections together with the neighboring basic reflection. (a) Low magnification; (b) higher magnification, clearly showing the shift occurring at the antiphase boundary.

values of the three reflections involved in the interference, and these will in general be different. The antiphase boundaries are now imaged as lines along which the fringes switch over from weak to strong or vice-versa, revealing a phase shift of π. Tilting the specimen did not move the "switch over line," which allows us to conclude that this line marks an interface and not an inclination contour. The switching over of the weak and strong lattice fringes occurs over a band of several unit cells wide. Such a width would be consistent with the assumption that the interface is inclined with respect to the beam. However, since the width remains fairly constant even when the orientation of the switch over line changes by roughly 90°, we suggest that the width reflects the band over which the order parameter changes in the boundary. This is consistent with the geometry since the projection of the Bi atom shifts is parallel to the fringe direction.

Heating the sample in the microscope with a focused electron beam causes a slight vibration of the antiphase boundaries over one or two lattice planes, but it does not alter the configuration.

DISCUSSION

As shown in (2) the paraelectric–antiferroelectric transition in $Bi_2Ti_4O_{11}$ is produced by parallel and antiparallel displacements of Bi atoms along the b direction resulting in an antiferroelectric polarization of the α-phase. In particular, since the (001) lattice fringes intersect the direction of the channels where the Bi atoms are placed, the broadening of the antiphase boundaries suggests that the change in the sense of displacement of the Bi atoms occurs gradually. The positions of the Bi ions along an antiferroelectric boundary are determined, on the one hand, by the tendency to remain in the equilibrium positions characteristic for the bulk α-phase (i.e., slightly eccentric within the oxygen octahedra forming the channel) and on the other hand, by the Coulomb repulsion. Along the antiphase boundaries the Bi atoms on the two sides of the boundary are displaced in opposite senses.

Before discussing a model of the gradual displacements of Bi atoms across the boundary, some remarks have to be made on the property of Bi^{3+} ions to have lone pairs or inert pairs (7, 8) giving rise to sometimes complicated structural deformations in a number of Bi^{3+}-oxygen compounds. The nonbonding lone pair is due to the hybridization of s and p orbitals. It is strongly stereoactive due to the eccentric space occupied by the associated electron cloud. The complicated structure adopted by even the simplest Bi^{3+} compounds can be attributed to the influence of such lone pairs on structural arrangements.

As deduced empirically from a number of structures

containing Bi^{3+} ions the Bi–O interatomic distances in the direction along the lone pair appear to fall in the range from 0.28 to 0.33 nm, whereas those in the other directions are significantly shorter and range from 0.22 to 0.26 nm. From the table of the interatomic distances in (2) we can clearly distinguish two categories of Bi–O separations in the α-$Bi_2Ti_4O_{11}$ compound. The first range from 0.317 to 0.337 nm; they are in the range mentioned above for lone pairs. The second class ranges frm 0.214 to 0.246 nm which is consistent with the second range. These values suggest that the lone pairs point presumably along the directions of the Bi–O(3) or Bi–O(2) segments (see Table IV in (2)).

In the paraelectric β-phase the lone pair electron clouds occupy random orientations with respect to the octahedral framework. On cooling, the lone pairs may gradually order, the space being occupied most economically if the lone pair electron clouds in a given channel point in the same direction. The strain of the TiO_6 network associated with this order may induce the formation of pairs of strings, presumably with opposite orientation of the lone pairs in neighboring channels. Such a transition, although associated with the cooperative orientational ordering of the lone pairs, is nevertheless displacive, since the final result is the ordered displacement of Bi atoms along the [010] direction. Since the ordering of lone pairs occurs rather gradually on lowering the temperature, the α–β transition is not sharp, which would explain the persistence of the weak superlattice reflections in the β-phase. The domain walls are rather mobile, a consequence of the relative ease of reorienting the lone pairs.

If we assume that in the α-phase the lone pair electron clouds are preferentially parallel and antiparallel to the [010] zone in the (b, c) plane, their gradual disordering on approaching the transition will cause a decrease of the b-parameter due to the randomization of the orientations. For the same reason the c-parameter would increase less than would follow from thermal expansion. The a-parameter will increase somewhat faster than by pure thermal expansion because on randomization the lone pair clouds leave the (b, c) plane. The randomization of the orientations of the lone pairs is also consistent with the variation of the lattice constants as function of temperature (6). In general the largest Bi–O separations in the α-phase decrease on going into the β-phase, whereas the reverse happens to the shortest Bi–O separations, i.e., the oxygen coordination of the Bi–ions becomes more regular.

With this model in mind, the structure of the antiphase boundaries can be derived. When a [010] channel is intersected by an antiphase boundary the displacements δ of the Bi-ions change sign; i.e., they are either both towards the boundary or both away from it. In the first case a local excess of Bi results; in the second case a local deficiency (see Fig. 8). The Coulomb interaction between the Bi^{3+} ions and their associated lone pair clouds will tend to widen the region over which the displacement switches from $+\delta$ to $-\delta$ or vice versa. One thus expects a boundary region to extend over a small number of unit cells. The excess or deficiency of Bi can be avoided if the boundary adopts an orientation belonging to the [010] zone since then the displacements δ are parallel to the interface. The antiphase boundary is then formed by a plane of adjacent channels along which the displacements are in the same sense. In fact the boundaries will meander adopting locally a low energy configuration at the expense of some lengthening; these features are visible in Fig. 7b where the boundary is wide and tends to be parallel to the fringes which mark the (001) planes.

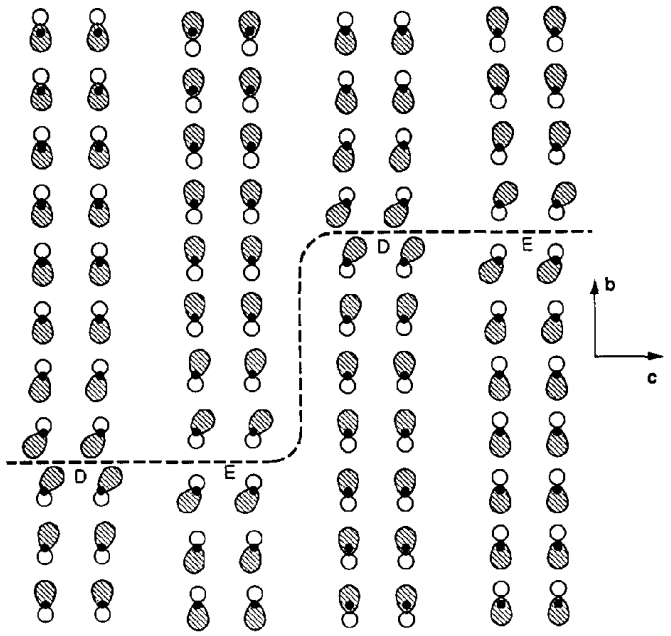

FIG. 8. Schematic structural model of an antiphase boundary in $Bi_2Ti_4O_{11}$; only the Bi configuration is represented. The hatched areas indicate the asymmetric lone pair. D refers to Bi-dense areas and E to Bi-poor areas.

There is a certain similarity in behavior between the present material and the Aurivillius phase $Bi_4Ti_3O_{12}$ which also contains Bi^{3+} ions coordinated by oxygen. This material becomes ferroelectric below 948 K. It is reasonable to assume that the origin of ferroelectricity in this compound should also be related to the ordering of lone pairs.

Pure Bi_2O_3 occurs in different forms: α is monoclinic, β is tetragonal, and γ is cubic. The α–β transition is at about 983 K. The deformation of the structures suggests that also in this case lone pairs play a role in determining the atom arrangement and in causing the transition by ordering.

ACKNOWLEDGMENT

L.N. acknowledges the Belgian Government, Prime Minister's Office of Science Policy Programming, for her fellowship at the University of Antwerp (RUCA).

REFERENCES

1. L. V. Petrushkova, S. P. Dimitrieva, E. V. Pobedimskaia, and N. V. Belov, *Sov. Phys. Dokl.* **19,** 263 (1974).
2. V. Kahlenberg and H. Böhm, *Acta Crystallogr. Sect. B* **51,** 11 (1995).
3. E. C. Subbarao, *J. Am. Ceram. Soc.* **45,** 564 (1962).
4. K. Hisano and K. Toda, *Solid State Commun.* **24,** 247 (1977).
5. L. V. Mitrovich and V. A. Blinov, *Fiz.-Khim. Issled. Strukt. Svoistv Stekol Steklokrist. Mater.* 18 (1982).
6. V. Kahlenberg and H. Böhm, *J. Phys.: Condens. Matter* **6,** 6221 (1994).
7. A. F. Wells, "Structural Inorganic Chemistry," p. 238. Clarendon, Oxford, 1975.
8. D. M. Adams, "Inorganic Solids. An Introduction to Concepts in Solid State Structural Chemistry," p. 130. Wiley, London, 1974.